

Supporting Information for

Optical Detection of Alcohols with a Cu(I)HETPHEN Complex by
Reversible Aldehyde to Hemiacetal Conversion

Lei Wang, Zhu-Lin Xie, Xin Li, Vincent Lynch, Karen L. Mulfort

General materials and methods. All reagents and solvents were purchased from commercial sources and used as received. 1,10-phenanthroline-4,7-dicarbaldehyde and 1,10-phenanthroline-2,9-dicarbaldehyde were prepared as pale-yellow needles (yield: 86.7%) according to the literature^[1] and their structure was confirmed by ¹H NMR ([Fig. S1-S2](#)). ¹H and ¹³C NMR were performed on a Bruker DMX 500 and referenced to TMS, TSP*, or the residual solvent peak. ESI-MS was collected on a ThermoFisher LCQ Fleet, from dilute methanol solutions in positive ionization mode. High-resolution mass spectrometry was performed at the University of Illinois School of Chemical Sciences Mass Spectrometry Laboratory (Champaign, IL, USA). Elemental analysis was performed by the Microanalysis Laboratory, School of Chemical Sciences, University of Illinois. UV-Vis absorption measurements were performed on a Beckman Coulter DU800 spectrophotometer.

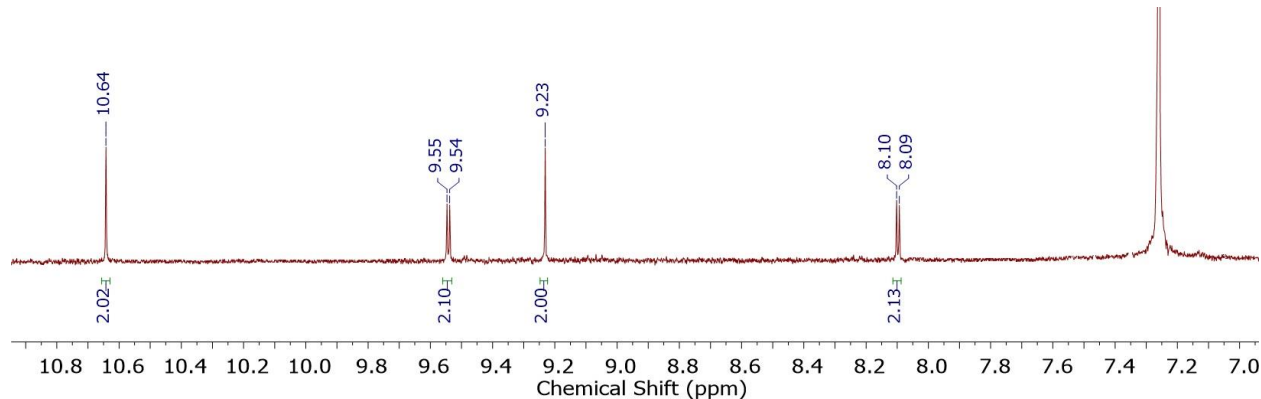


Fig. S 1. ¹H NMR spectrum for 1,10-phenanthroline-4,7-dicarbaldehyde in chloroform-*d*.

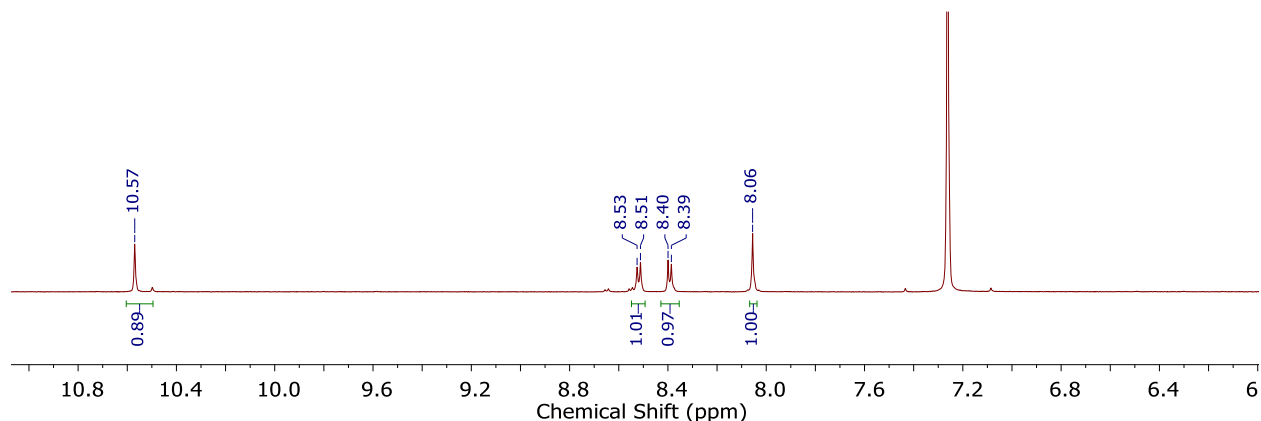


Fig. S 2. ¹H NMR spectrum for 1,10-phenanthroline-2,9-dicarbaldehyde in chloroform-*d*.

Synthetic procedures

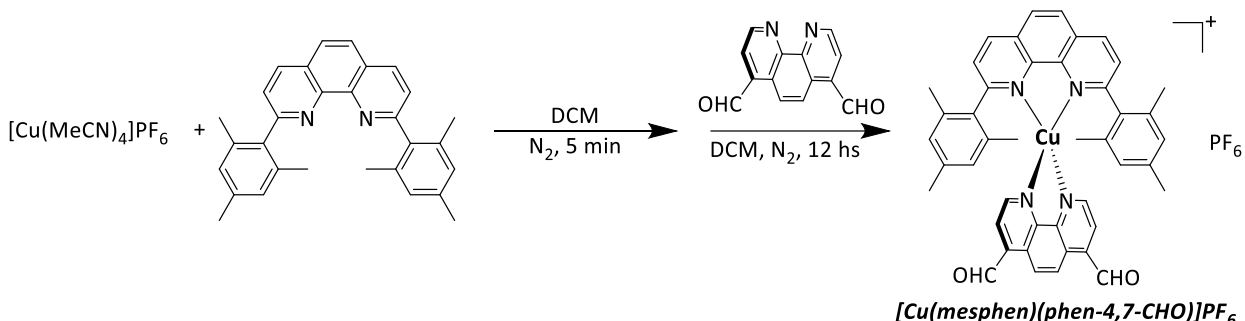


Fig. S3. Synthesis of complexes **Cu-4,7-CHO**, i.e. $[\text{Cu}(\text{mesphen})(\text{phen-4,7-CHO})]\text{PF}_6$.

The complexes reported here exploit the HETPHEN strategy^[2], which yield to a relatively stable copper complex with respect to other Cu(I)diamine complexes. Detailed synthetic procedures and characterization are described in the Supporting Information. Aldehyde group was introduced with 4,7-dimethyl-1,10-phenanthroline in the existence of selenium dioxide in 1,4-dioxane. The copper complex was prepared by the one-pot, two-step synthesis procedure at room temperature using dichloromethane as the solvent as previously described^[3].

Complex Cu-4,7-CHO. The synthesis of the target complex, $[\text{Cu}(\text{mesphen})(4,7\text{-CHO-phen})]\text{PF}_6$ (where mesphen = 2,9-dimesityl-1,10-phenanthroline and 4,7-CHO-phen = 4,7-aldehyde-1,10-phenanthroline), was proceeded by the same procedure as we submitted recently^[3].

¹H NMR (500 MHz, Acetone-*d*₆, Fig. S4) δ 10.81 (s, 2H), 9.30 – 9.25 (m, 4H), 9.00 (d, *J* = 8.2 Hz, 2H), 8.53 (d, *J* = 4.8 Hz, 2H), 8.44 (s, 2H), 8.05 (d, *J* = 8.2 Hz, 2H), 6.02 (s, 4H), 1.81 (s, 12H), 1.56 (s, 6H). ¹³C NMR (126 MHz, Acetone-*d*₆, Fig. S5) δ 193.29, 159.79, 149.94, 144.76, 144.06, 138.69, 138.25, 137.30, 135.42, 129.72, 128.81, 127.50, 125.94, 125.71, 20.45, 20.08. ESI-MS C₄₄H₃₆CuN₄O₂⁺ calcd 715.21; found 715.33. HRMS ESI C₄₄H₃₆N₄O₂Cu⁺ calcd 715.2136 found 715.2134. Elemental Analysis (calcd., found for C₄₄H₃₆N₄O₂CuF₆P·1/5CH₂Cl₂): C (61.74, 60.44), H (4.78, 4.08), N (6.65, 6.36).

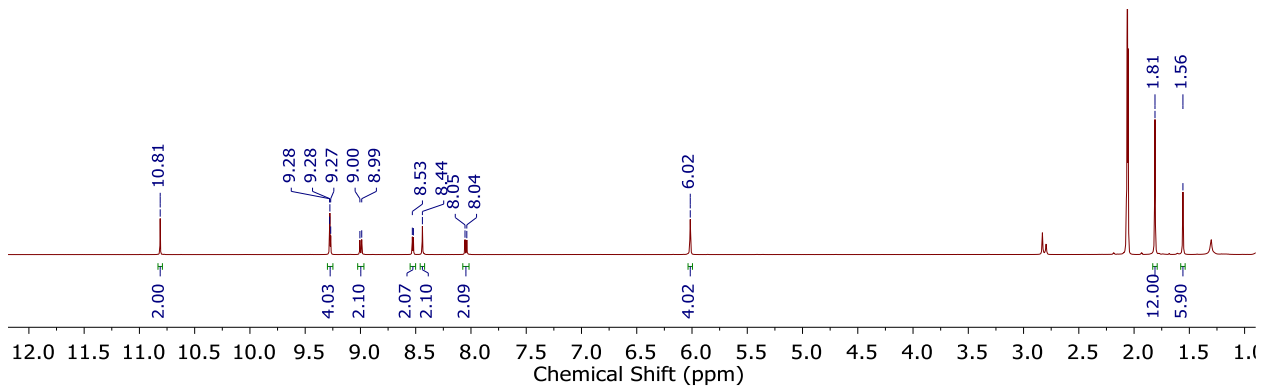


Fig. S4. ^1H NMR spectrum for complex **Cu-4,7-CHO** in acetone- d_6 .

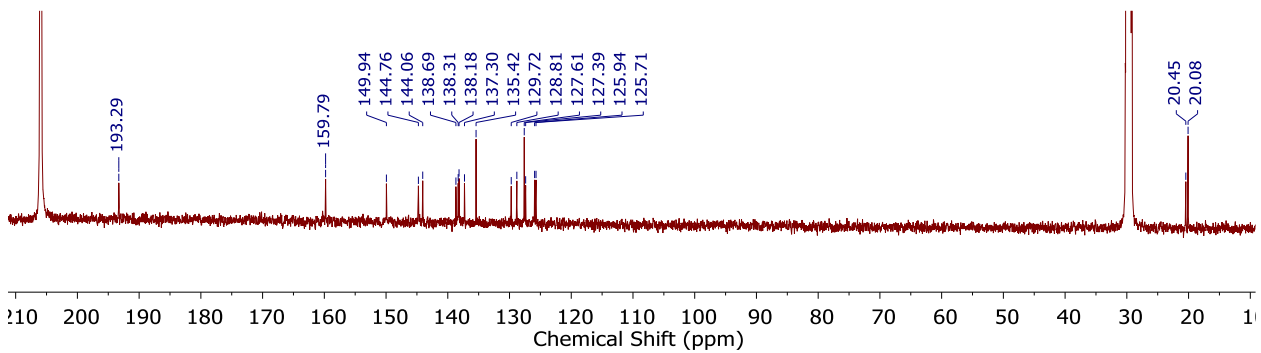


Fig. S5. ^{13}C NMR spectrum for complex **Cu-4,7-CHO** in acetone- d_6 .

Complex Cu-4,7-HA (R=HC(OH)(OCH₃)). ^1H NMR (500 MHz, Methanol- d_4 , Fig. S6) δ 8.78 (d, $J = 8.1$ Hz, 2H), 8.55 (d, $J = 4.6$ Hz, 2H), 8.25 (d, $J = 8.2$ Hz, 4H), 7.99 – 7.80 (m, 4H), 6.19 (s, 2H), 5.95 (dd, $J = 19.7$, 14.7 Hz, 4H), 1.70 (t, $J = 12.3$ Hz, 12H), 1.56 (s, 6H). ^{13}C NMR (500 MHz, Methanol- d_4 , Fig. S7) δ 159.81, 148.66, 147.43, 144.47, 144.09, 138.26, 137.97, 135.07, 128.68, 127.52, 127.19, 126.56, 123.77, 121.83, 95.04, 20.13, 19.72. ESI-MS C₄₆H₄₄CuN₄O₄⁺ calcd 779.27; found 779.50. HRMS ESI C₄₆H₄₄CuN₄O₄⁺ calcd 779.2659 found 779.2667.

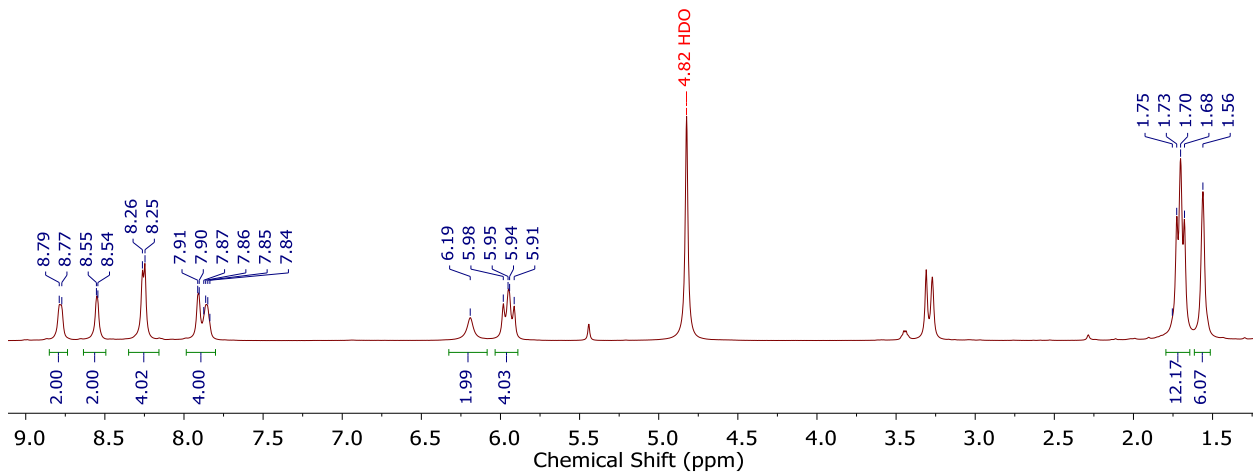


Fig. S 6. ^1H NMR spectrum for complex **Cu-4,7-HA** in methanol- d_4 .

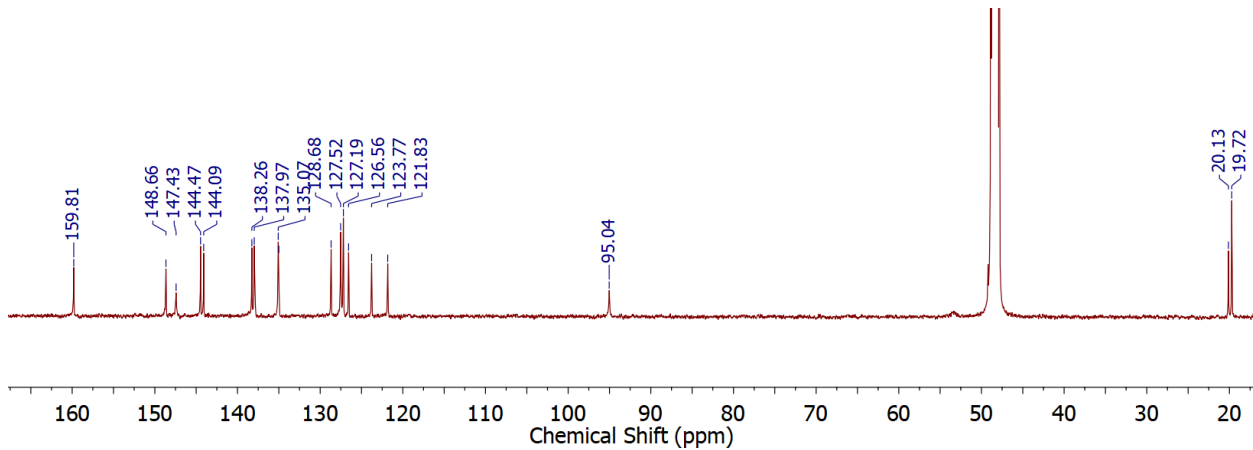


Fig. S 7. ^{13}C NMR spectrum for complex **Cu-4,7-HA** in methanol- d_4 .

Complex Cu-2,9-CHO. ^1H NMR (500 MHz, Acetone- d_6 , Fig. S8) δ 10.15 (s, 2H), 9.10 (d, $J = 8.2$ Hz, 2H), 9.02 (d, $J = 8.2$ Hz, 2H), 8.55 – 8.44 (m, 6H), 8.09 (d, $J = 8.2$ Hz, 2H), 5.98 (s, 4H), 1.60 (d, $J = 12.5$ Hz, 18H). ^{13}C NMR (500 MHz, Acetone- d_6 , Fig. S9) δ 190.35 , 158.93 , 144.14 , 138.88 , 138.39 , 137.64 , 134.57 , 132.20 , 129.38 , 128.57 , 126.97 , 126.80 , 123.29 , 19.66 , 19.44 .

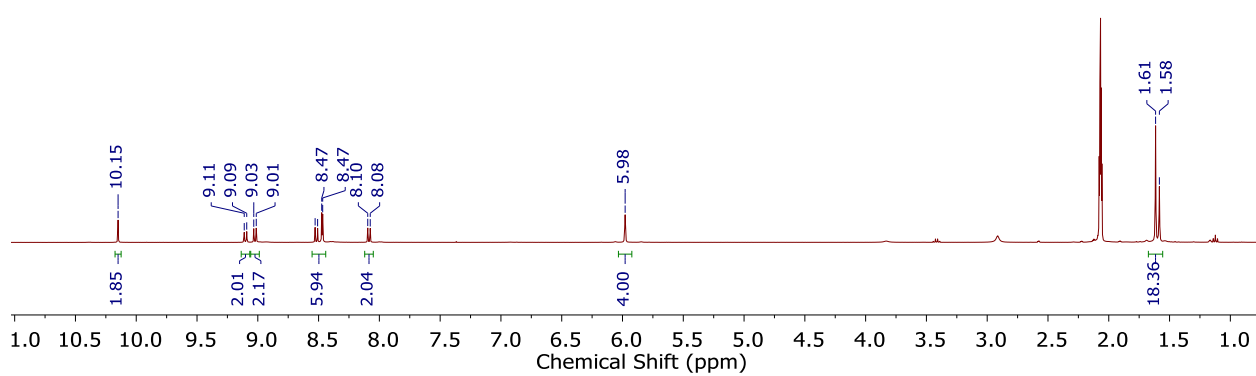


Fig. S 8. ¹H NMR spectrum for complex **Cu-2,9-CHO** in acetone-*d*₆.

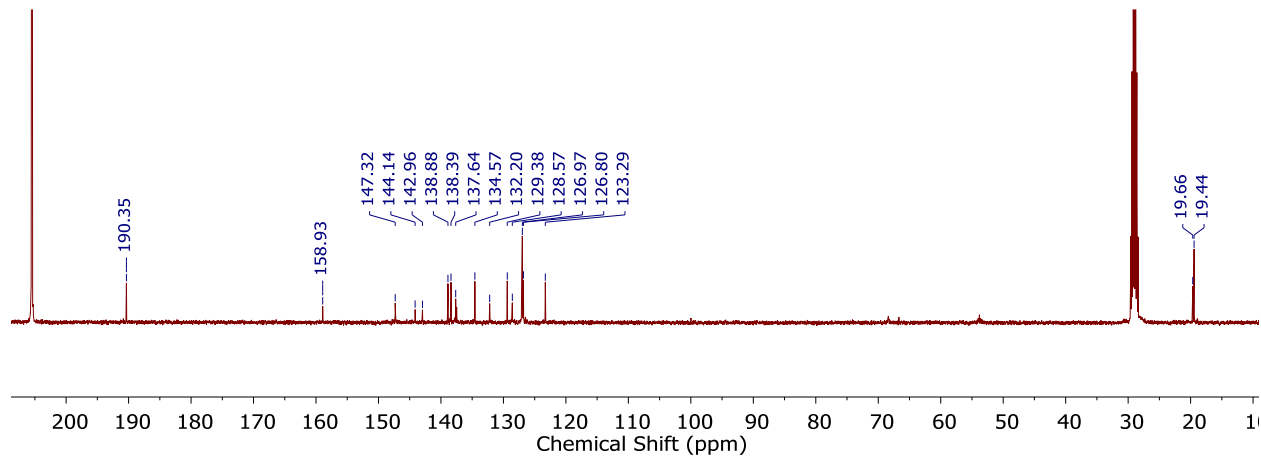


Fig. S 9. ¹³C NMR spectrum for complex **Cu-2,9-CHO** in acetone-*d*₆.

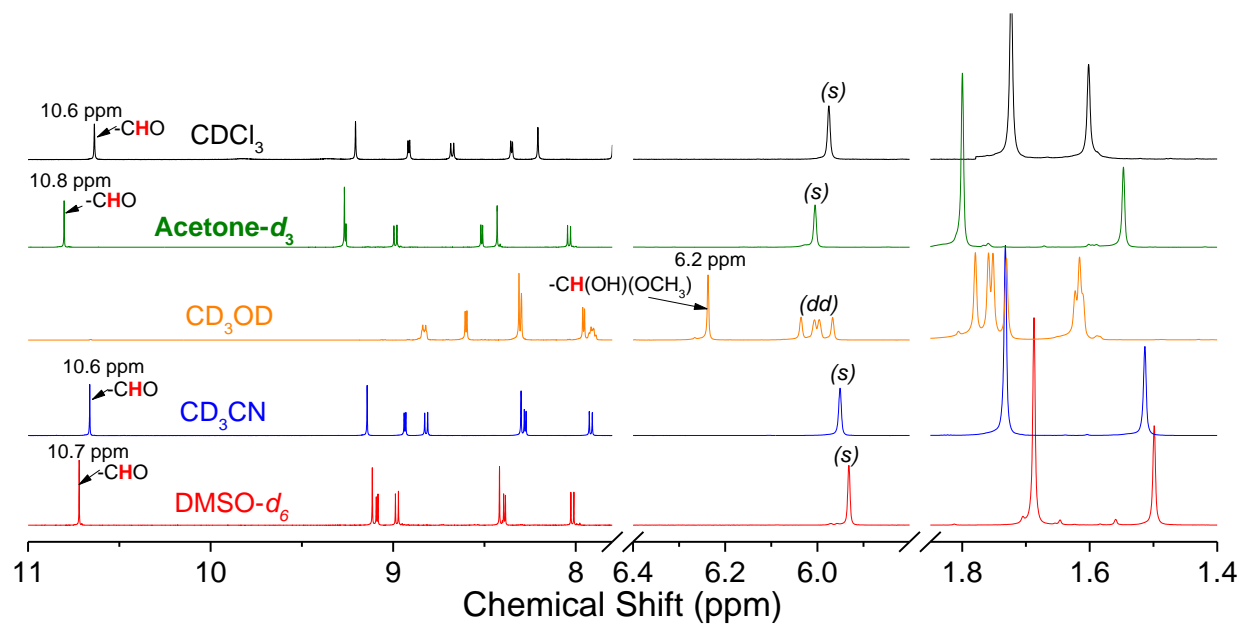


Fig. S 10. ¹H NMR spectrum for **Cu-4,7-CHO** in different solvents.

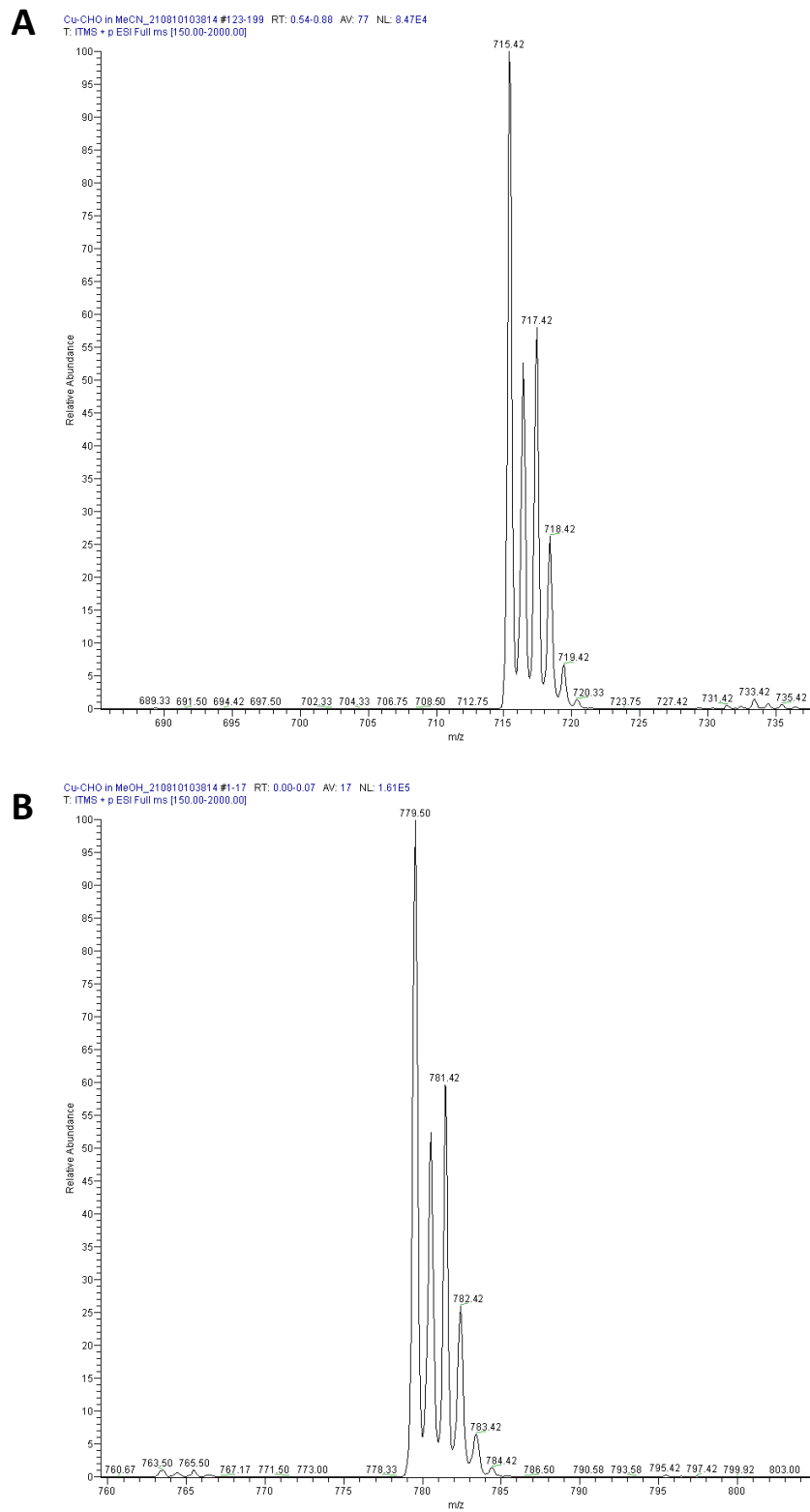


Fig. S 11. Mass spectrum of **Cu-4,7-CHO** (top) in MeCN and **Cu-4,7-HA** (bottom) in MeOH.

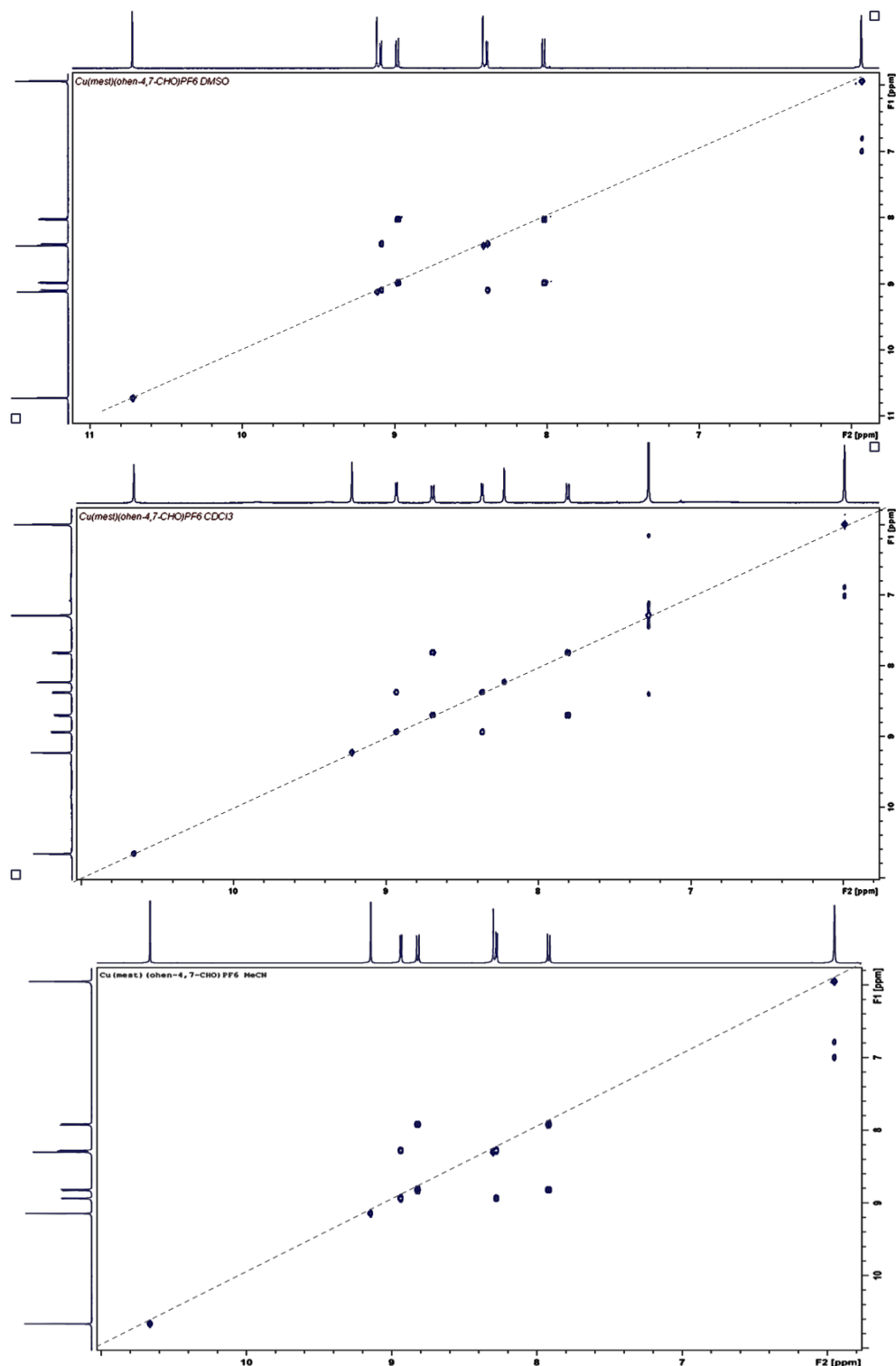


Fig. S 12. 2D ^1H - ^1H COSY spectra of the complex in DMSO (top), CDCl₃ (middle), and CD₃CN (bottom).

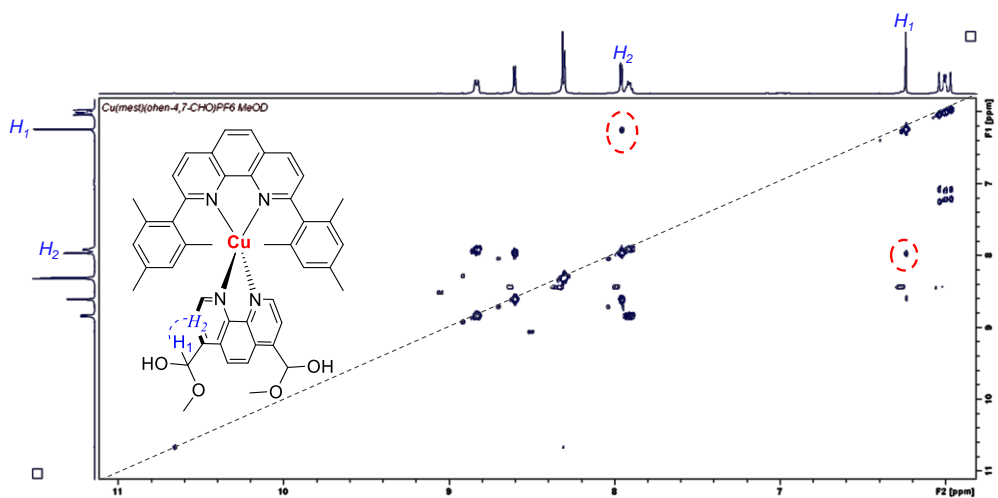


Fig. S 13. 2D ^1H - ^1H COSY spectra of **Cu-4,7-CHO** in methanol- d_4 .

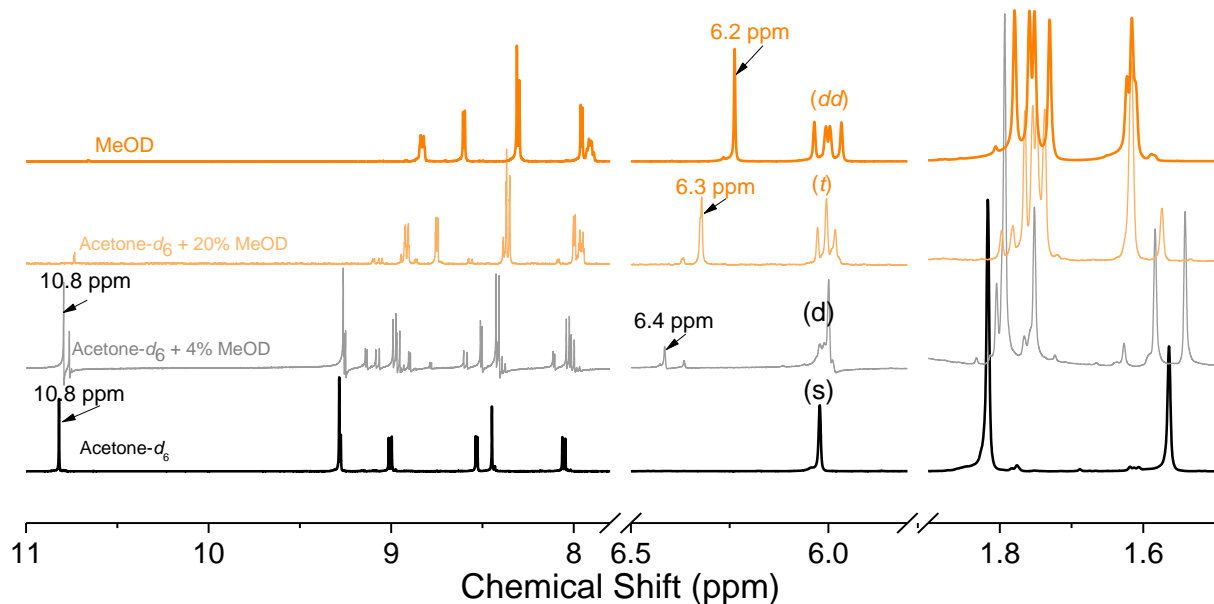


Fig. S 14. ^1H NMR spectrum for **Cu-4,7-CHO** in acetone- d_6 with adding different amounts of methanol- d_4 .

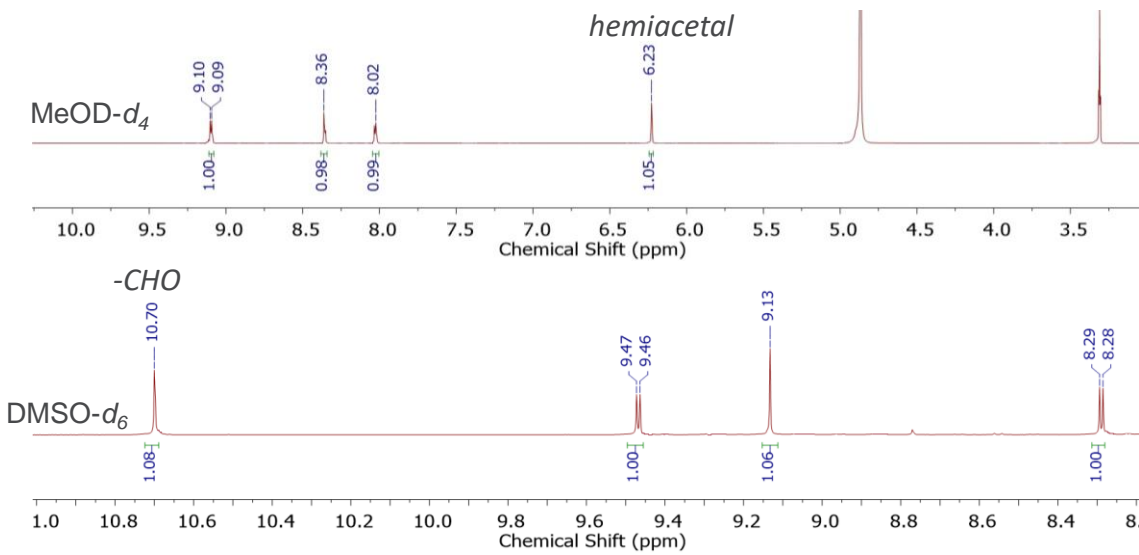


Fig. S 15. ¹H NMR spectrum for ligand **phen-4,7-CHO** in methanol-*d*₄ (top) and in DMSO-*d*₆ (bottom).

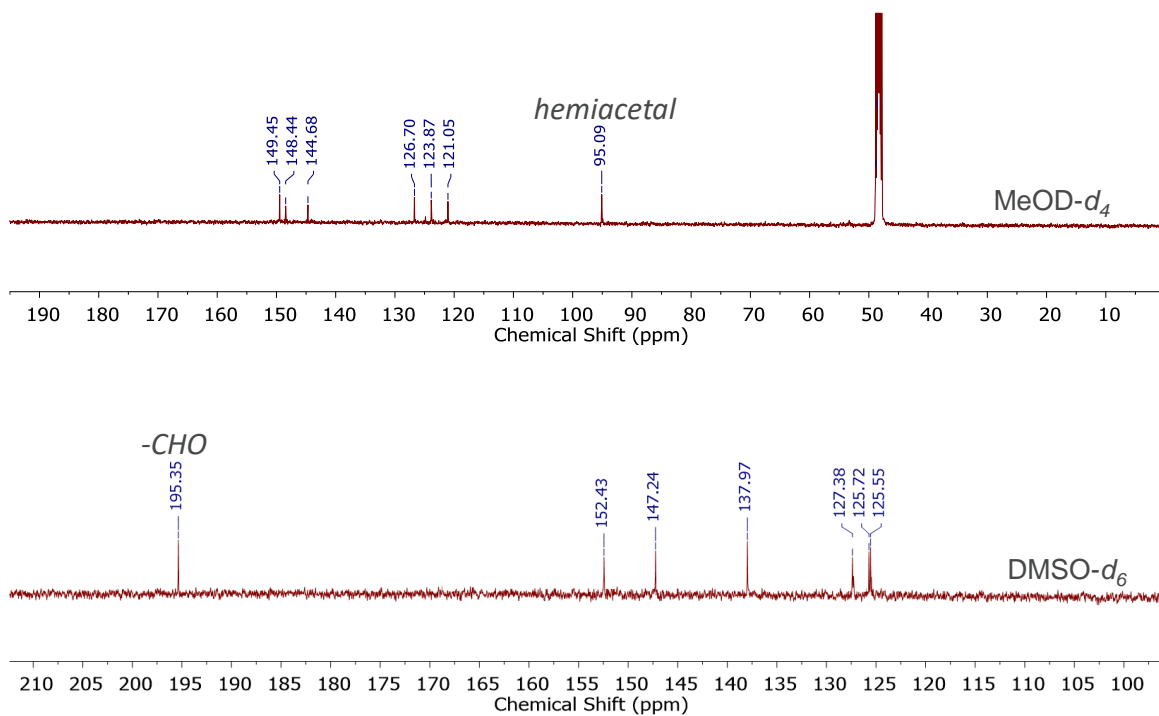


Fig. S 16. ¹³C NMR spectrum for ligand **phen-4,7-CHO** methanol-*d*₄ (top) and in DMSO-*d*₆ (bottom).

Crystallography

Single crystal data was collected at the University of Texas at Austin Faulkner Nanoscience and Technology Center, Department of Chemistry, X-ray Diffraction Lab. The structures were solved by direct methods using SHELXT^[4] and refined by full-matrix least-squares on F^2 with anisotropic displacement parameters for the non-H atoms using SHELXL-2018/3.^[5] Structure analysis was aided by use of the programs PLATON^[6] and OLEX2.^[7] The hydrogen atoms bound to carbon atoms were calculated in idealized positions. Definitions used for calculating $R(F)$, $R_w(F^2)$ and the goodness of fit, S , are given below:

$$R_w(F^2) = [\sum w(|F_o|^2 - |F_c|^2)^2 / \sum w(|F_o|)^4]^{1/2}, \text{ where } w \text{ is the weight given each reflection.}$$

$$R(F) = \sum (|F_o| - |F_c|) / \sum |F_o|, \text{ for reflections with } F_o > 4(\sigma(F_o)).$$

$$S = [\sum w(|F_o|^2 - |F_c|^2)^2 / (n - p)]^{1/2}, \text{ where } n \text{ is the number of reflections and } p \text{ is the number of refined parameters.}$$

The data were checked for secondary extinction but no correction was necessary. Neutral atom scattering factors and values used to calculate the linear absorption coefficient are from the International Tables for X-ray Crystallography (1992).^[8] All Fig.s were generated using SHELXTL/PC.^[9]

Cu-4,7-CHO ($[(C_{30}H_{28}N_2)Cu(C_{14}H_8N_2O_2]PF_6 \cdot CH_2Cl_2$): Crystals grew as clusters of reddish prisms by slow evaporation from dichloromethane and diethyl ether^[3]. The crystal used for data collection was separated from a cluster of crystals and had approximate dimensions; 0.20 x 0.10 x 0.04 mm. The data were collected on an Agilent Technologies SuperNova Dual Source diffractometer using a μ -focus Cu K α radiation source ($\lambda = 1.5418\text{\AA}$) with collimating mirror monochromators. A total of 980 frames of data were collected using ω -scans with a scan range of 1° and a counting time of 13.5 seconds per frame for frames collected with a detector offset of -41.6° and 52 seconds per frame with frames collected with a detector offset of 107.1° . The data were collected at 100 K using an Oxford Cryostream low temperature device. Details of crystal data, data collection and structure refinement are listed in Table S1. Data collection, unit cell refinement and data reduction were performed using Rigaku Oxford Diffraction's CrysAlicPro Software System (2019), 1.171.41.70a. The function, $\sum w(|F_o|^2 - |F_c|^2)^2$, was minimized, where

$w = 1/[(\sigma(F_o))^2 + (0.0632 * P)^2 + (4.1244 * P)]$ and $P = (|F_o|^2 + 2|F_c|^2)/3$. $R_w(F^2)$ refined to 0.118, with R(F) equal to 0.0407 and a goodness of fit, S = 1.05.

Cu-4,7-HA ($[(C_{30}H_{28}N_2)Cu(C_{16}H_{16}N_2O_4]PF_6$): Crystals grew as red plates by vapor diffusion of pentane into a methanol solution. The crystal used for data collection was separated from a cluster of crystals and had approximate dimensions; 0.29 x 0.13 x 0.07 mm. Rigaku Oxford Diffraction HyPix6000E Dual Source diffractometer using a μ -focus Cu K α radiation source ($\lambda = 1.5418\text{\AA}$) with collimating mirror monochromators. A total of 1722 frames of data were collected using ω -scans with a scan range of 0.5° and a counting time of 4 seconds per frame for frames collected with a detector offset of +/- 48.3° and 16 seconds per frame with frames collected with a detector offset of +/- 105.1°. The data were collected at 100 K using an Oxford Cryostream low temperature device. Details of crystal data, data collection and structure refinement are listed in Table S1. Data collection, unit cell refinement and data reduction were performed using Rigaku Oxford Diffraction's CrysAlicPro Software System (2019), 1.171.41.115a. The function, $\sum w(|F_o|^2 - |F_c|^2)^2$, was minimized, where $w = 1/[(\sigma(F_o))^2 + (0.0763 * P)^2 + (2.9839 * P)]$ and $P = (|F_o|^2 + 2|F_c|^2)/3$. $R_w(F^2)$ refined to 0.167, with R(F) equal to 0.0605 and a goodness of fit, S = 1.18.

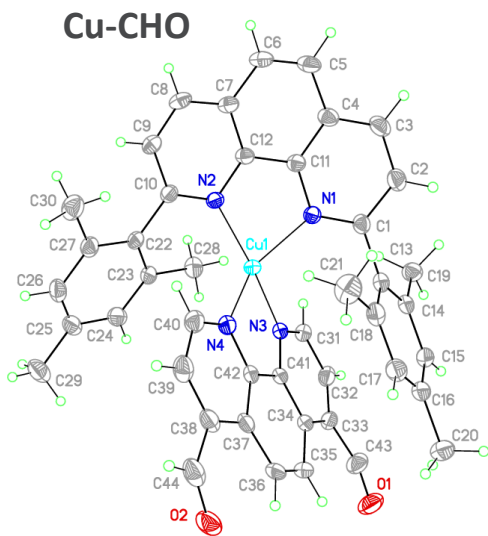


Fig. S 17. View of the Cu ion complex in **Cu-4,7-CHO** showing the atom labeling scheme. Displacement ellipsoids are scaled to the 50% probability level.

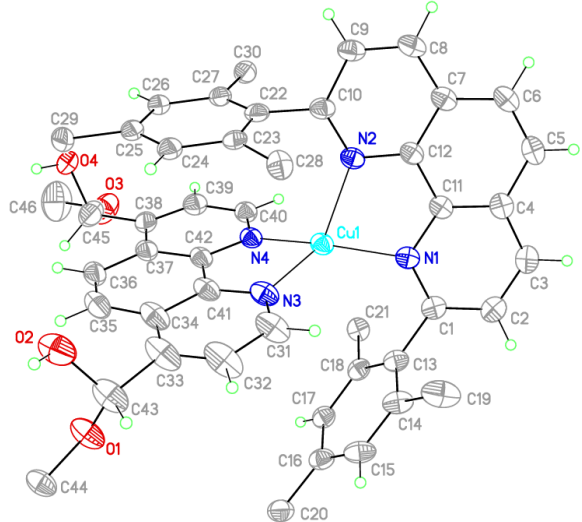


Fig. S 18. View of the Cu complex in **Cu-4,7-HA** showing the atom labeling scheme. Displacement ellipsoids are scaled to the 30% probability level. The methyl H atoms were omitted for clarity. The lower occupancy atoms of the disordered groups were omitted from view.

Table S 1. Details of crystal structure refinement of complexes Cu-X.

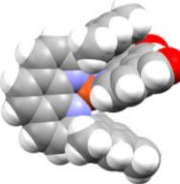
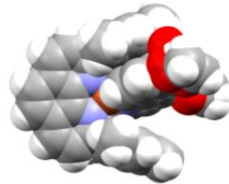
Complex	Cu-4,7-CHO	Cu-4,7-HA
CCDC #	2226034	2226033
Space-filling diagrams		
Formula	$C_{46.50}H_{38}Cl_2CuF_6N_4O_2P$	$C_{46}H_{44}CuF_6N_4O_4P$
Mw (g/mol)	964.22	925.14
Lattice type	monoclinic	monoclinic
Space group	P 1 21/n 1	P 1 21/n 1
a (Å)	13.52666(16)	14.7098(2)
b (Å)	18.9337(2)	20.7473(3)
c (Å)	17.8755(3)	14.7414(3)
$\alpha(^{\circ})$	90	90
$\beta(^{\circ})$	106.542(13)	104.9231(17)
$\gamma(^{\circ})$	90	90
V (Å ³)	4388.59(10)	4347.18(12)
Z	4	4
ρ_{calc} (g cm ⁻¹)	1.459	1.414
T (K)	100.02(13)	100.00(18)
λ (Å) [Mo K α]	1.54184	1.54184
μ (mm ⁻¹)	2.764	1.694
S (GOF)	1.046	1.179
R(Fo), wR(Fo ²)	0.0407, 0.1125	0.0605, 0.1633

Table S 2. Selected Bond Length, Bond Angles, and Geometry Index Parameter s_4 .

Complex	Cu-4,7-CHO	Cu-4,7-HA
Selected bond length		
Cu–N1	2.057(2)	1.996(2)
Cu–N2	2.008(2)	2.071(2)
Cu–N3	2.027(2)	2.012(3)
Cu–N4	2.025(2)	2.032(2)
Selected bond angles		
N1–Cu–N2	83.13(7)	82.21(9)
N1–Cu–N3	113.72(7)	128.40(11)
N1–Cu–N4	116.69(7)	134.08(9)
N2–Cu–N3	136.80(7)	124.84(9)
N2–Cu–N4	127.37(7)	109.51(9)
N3–Cu–N4	82.00(7)	82.06(10)
s_4 values	0.680	0.692

Computational methods. Density functional theory (DFT) calculations of CuHETPHEN complexes were performed using Gaussian 16, revision C.01.^[10] Geometry optimization was achieved with the functional of B3LYP.^[11] The basis set of LANL2DZ with effective core potential (ECP)^[12] was used for Cu and 6-31G(d,p)^[13] for all other atoms. Frequency calculations were performed at the same level of theory to confirm the nature of stationary points with non-imaginary points for the minima. Solvent corrections (dichloromethane and methanol) were included through polarizable continuum model using the integral equation formalism variant (IEFPCM).^[14] Calculations were performed without considering the effect of anion since they are the same PF₆. Predicted electronic transitions were calculated using time-dependent DFT (TD-DFT) calculations at B3LYP level with LANL2DZ (ECP) for Cu and 6-31G+(d,p) for all other atoms. Orbital surfaces and simulated spectra were generated from the GaussView program (version 5.0.9).^[15] Natural transition orbital (NTO) analysis^[16] was carried out using Multiwfn program.^[17]

Table S 3. UV-vis spectrum of copper complexes in different solvents.

Complex	Solvents	λ_{max} (MLCT, nm)	Molar Extinction Coefficients (ϵ , $\text{M}^{-1}\text{cm}^{-1}$)
Cu-4,7-HA	Methanol	467	7790
Cu-4,7-CHO	Dichloromethane	422, 530	5007, 6627
Cu-4,7-CHO	Acetone	428, 525	3728, 5212
Cu-4,7-CHO	DMF	431, 519	4036, 4615
Cu-4,7-CHO	Acetonitrile	423, 527	5484, 7434

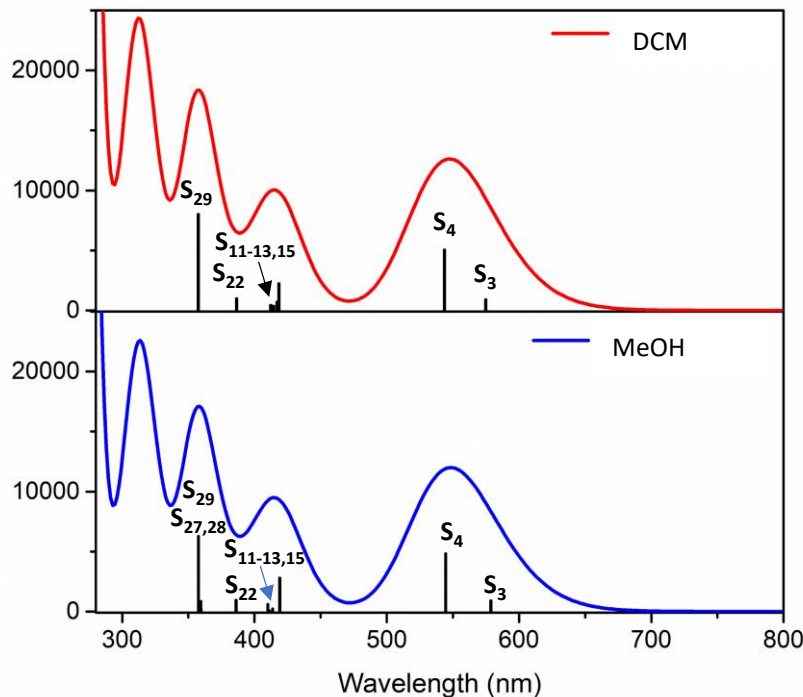


Fig. S 19. Comparison of the theoretical spectra for complex **Cu-4,7-CHO** in dichloromethane (red) and in methanol (blue).

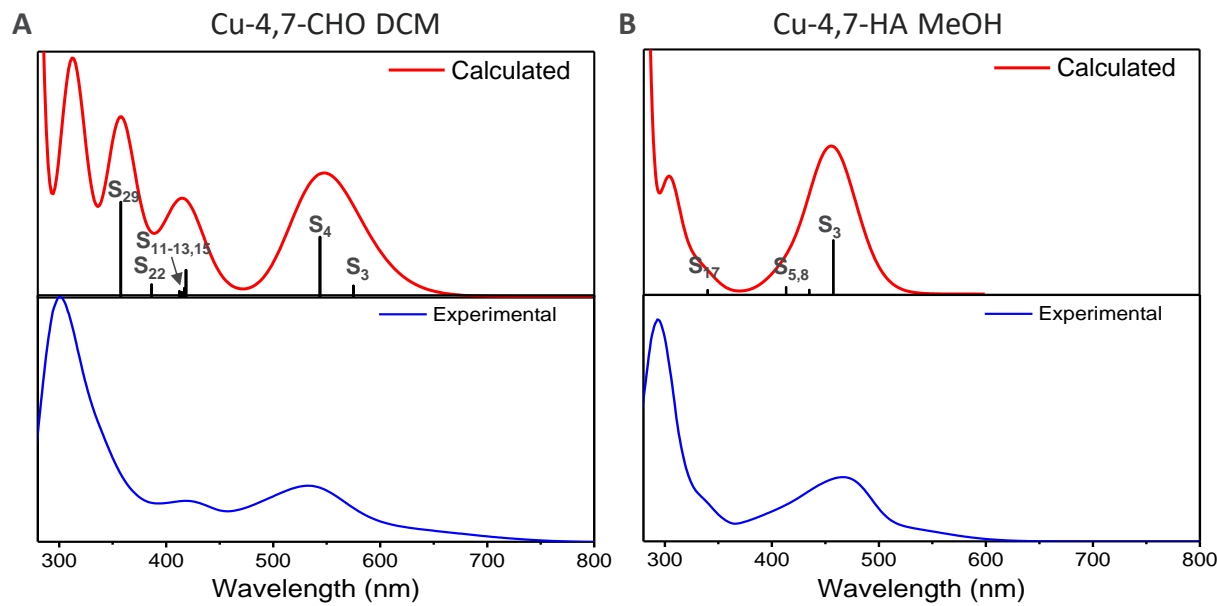


Fig. S 20. Comparison of the theoretical (red) and experimental (blue) spectra for complex (A) **Cu-4,7-CHO** in dichloromethane and (B) **Cu-4,7-HA** in methanol.

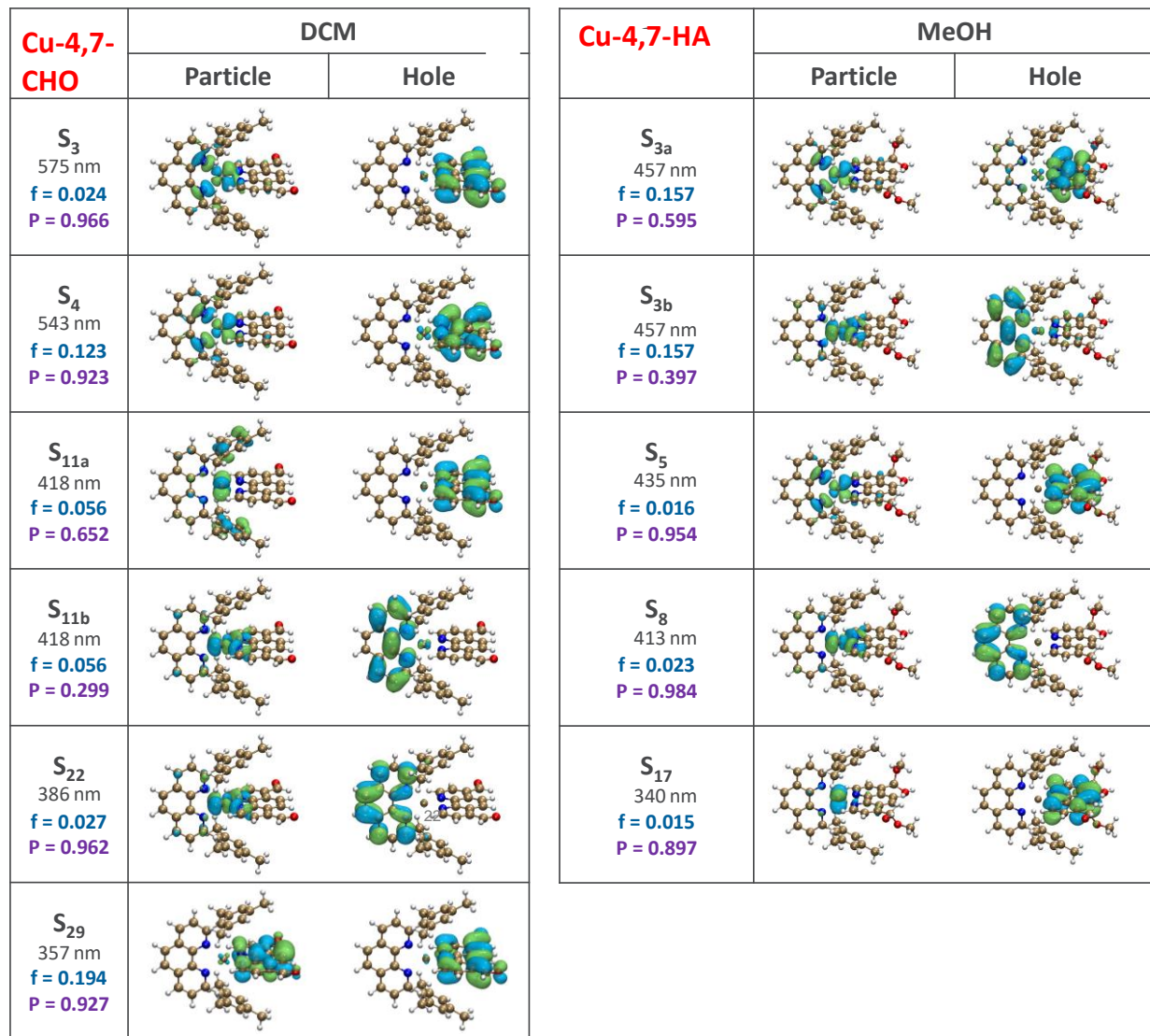


Fig. S 21. Natural Transition Orbitals (NTO) of **Cu-4,7-CHO** in DCM (left) and **Cu-4,7-HA** in MeOH (right) by TDDFT calculations.

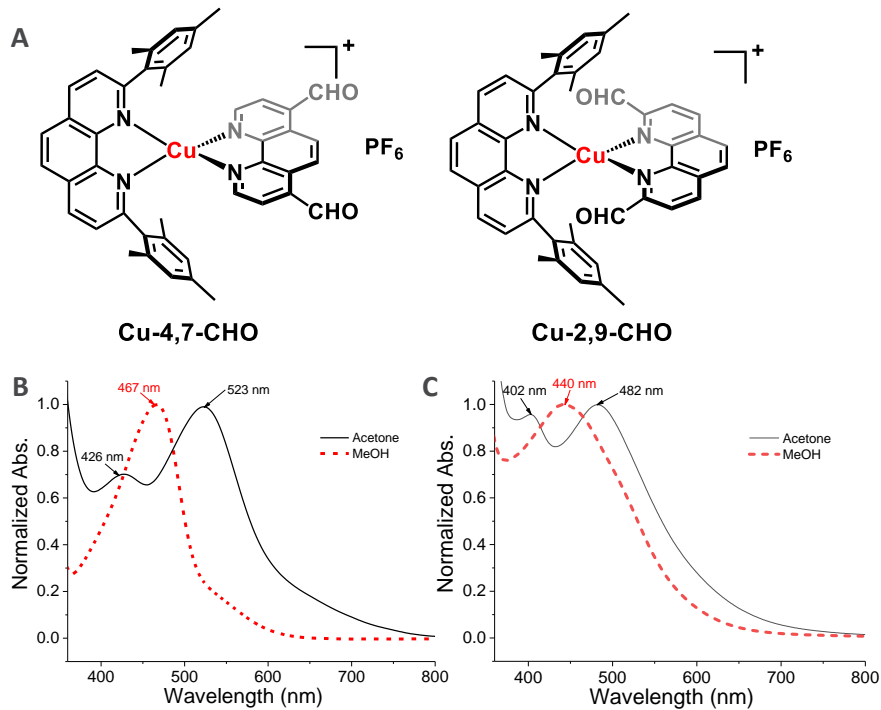


Fig. S 22. (A) Chemical structure of **Cu-4,7-CHO** and **Cu-2,9-CHO** complexes. (B, C) UV-vis absorption spectra for (B) complex **Cu-4,7-CHO/Cu-4,7-HA** and (C) complex **Cu-2,9-CHO/Cu-2,9-HA** in acetone (solid, black) and methanol (dash, red).

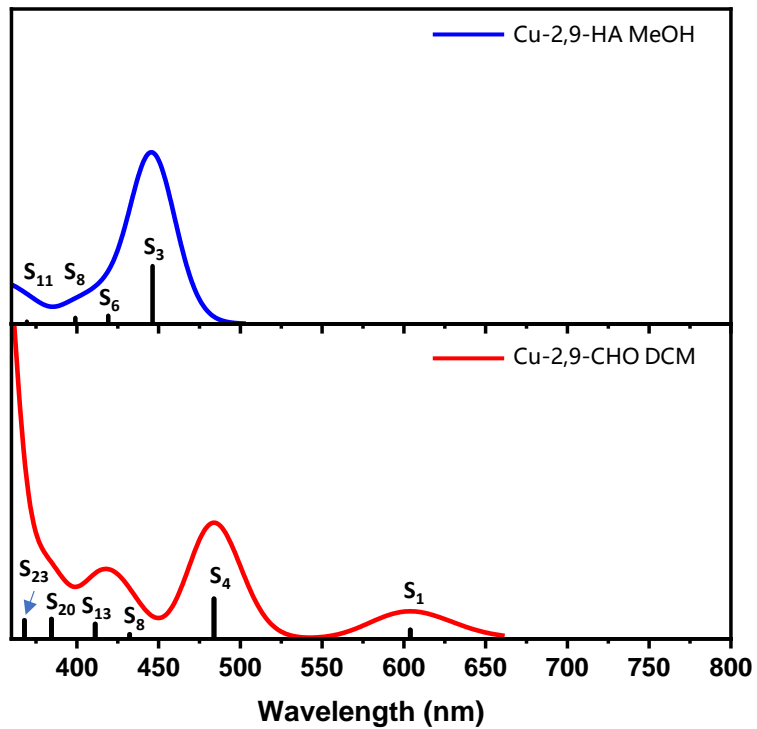


Fig. S 23. Comparison of the theoretical spectra for complex **Cu-2,9-HA** in methanol (blue) **Cu-2,9-CHO** in dichloromethane (red).

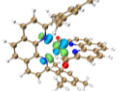
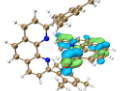
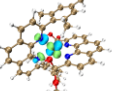
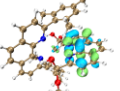
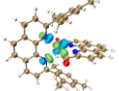
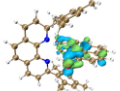
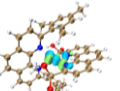
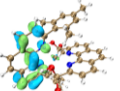
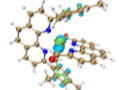
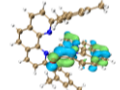
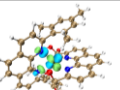
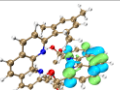
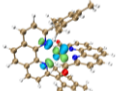
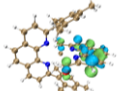
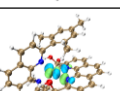
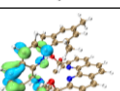
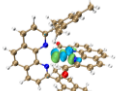
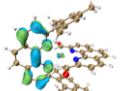
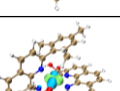
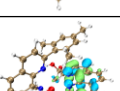
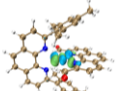
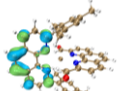
Cu-2,9-CHO	DCM		Cu-2,9-HA	MeOH	
	Particle	Hole		Particle	Hole
S₁ 604 nm $f = 0.0129$ $P = 0.990218$			S_{3a} 446 nm $f = 0.0786$ $P = 0.559724$		
S₄ 484 nm $f = 0.0547$ $P = 0.922299$			S_{3b} 446 nm $f = 0.0786$ $P = 0.407323$		
S₈ 432 nm $f = 0.0068$ $P = 0.95529$			S₆ 419 nm $f = 0.0116$ $P = 0.954961$		
S₁₃ 411 nm $f = 0.0207$ $P = 0.929566$			S₈ 399 nm $f = 0.0086$ $P = 0.97972$		
S₂₀ 384 nm $f = 0.0273$ $P = 0.869907$			S₁₁ 369 nm $f = 0.0035$ $P = 0.828396$		
S₂₃ 368 nm $f = 0.0256$ $P = 0.958891$					

Fig. S 24. Natural Transition Orbitals (NTO) of **Cu-2,9-CHO** in DCM (left) and **Cu-2,9-HA** in MeOH (right) by TDDFT calculations.

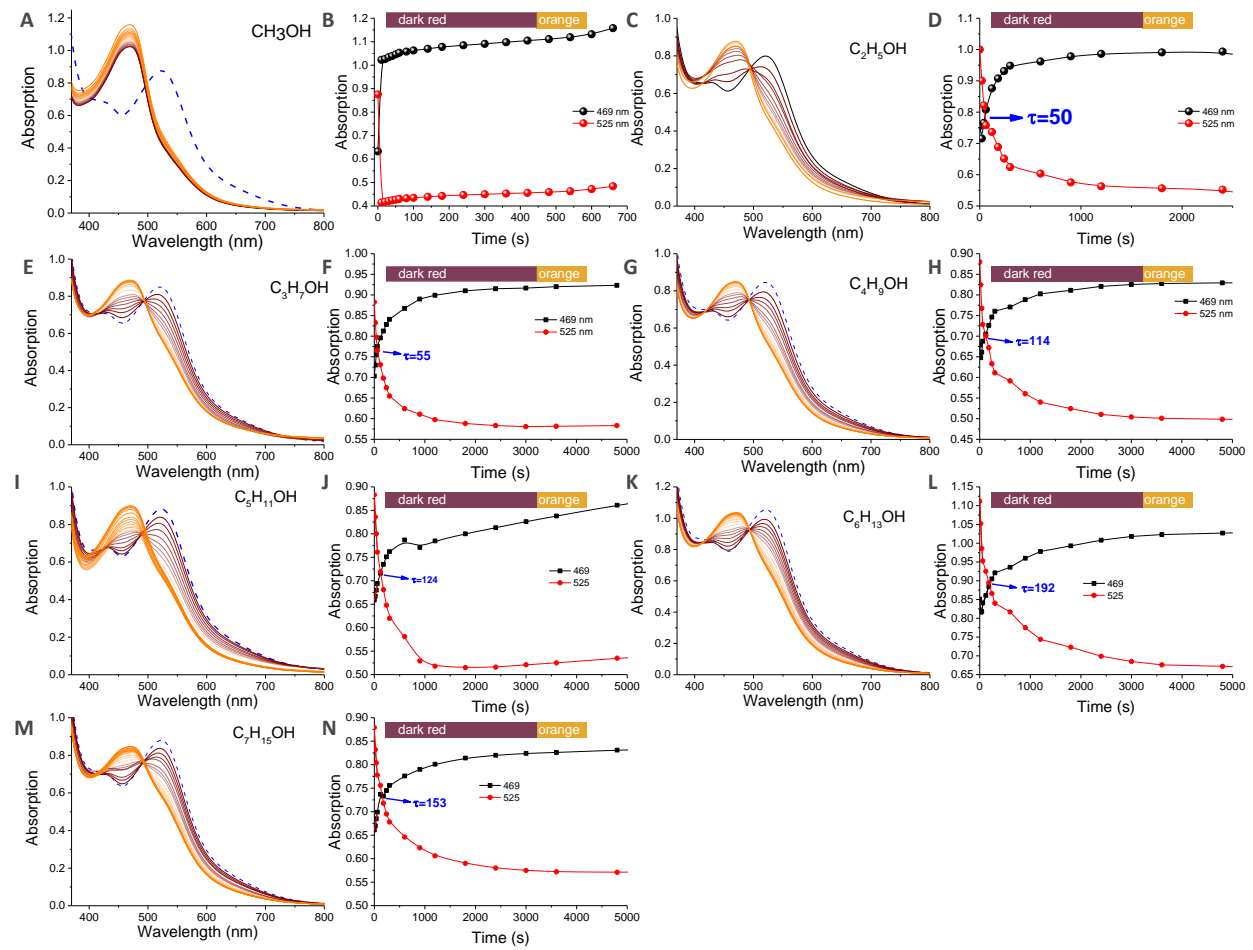


Fig. S 25. UV spectrum titration of 500 μM complexes **Cu-4,7-CHO** in acetone with adding different alcohols.

Table S4. Properties of different alcohols in this study and the response time.

Alcohols	Viscosity ^[a]	D ⁰ /10 ⁻⁵ [b]	Polar substituent constant (σ*) ^[c]	Steric substituent constant (Es) ^[c]	τ ^[d] (s)	k (s ⁻¹)
Methanol	0.51	1.54	0	0.00	<1	1
Ethanol	0.99	1.22	-0.1	-0.07	50	0.02
1- Propanol	1.73	1.05	-0.12	-0.36	55	0.01818
1-Butanol	2.26	0.96	-0.13	-0.39	114	0.00877
1- Pentanol	3.05	0.88	/	-0.40	124	0.00806
1-Hexanol	3.86	0.83	/	/	192	0.005208
1- Heptanol	5.03	0.80	/	/	153	0.006536

[a] Viscosities of these alcohols at room temperature (30°C) at 1Kpa (unit: mPa·s). Data from reference^[18]; [b] Diffusion coefficients (D^0) of these alcohols in air at room temperature (25°C) (unit: cm²/s). Data from reference^[19]; [c] Data from reference^[20]; [d] Cross point of the absorption response to time.

$$\text{Taft equation: } \log \frac{k}{k_{\text{CH}_3}} = \sigma^* \times \rho^* + \delta E_s$$

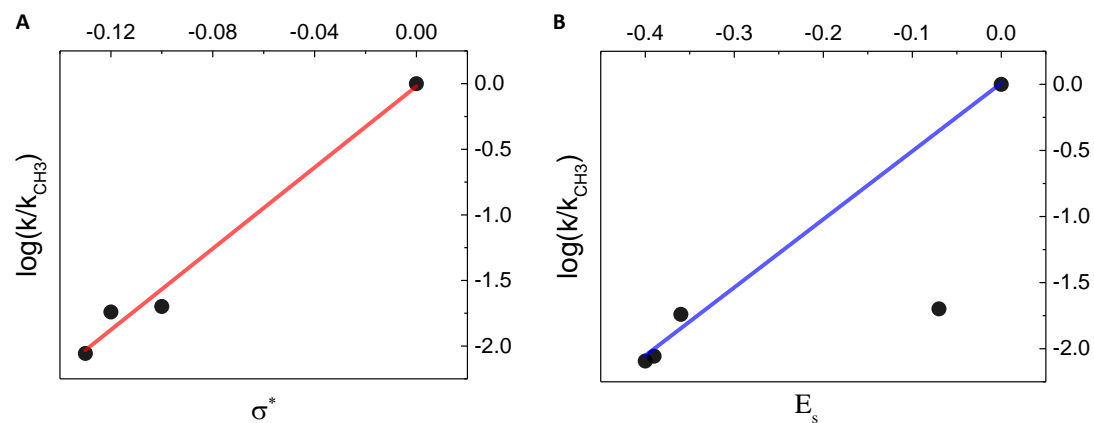


Fig. S26. Taft relationship for increased alkyl chain lengths in alcohols.

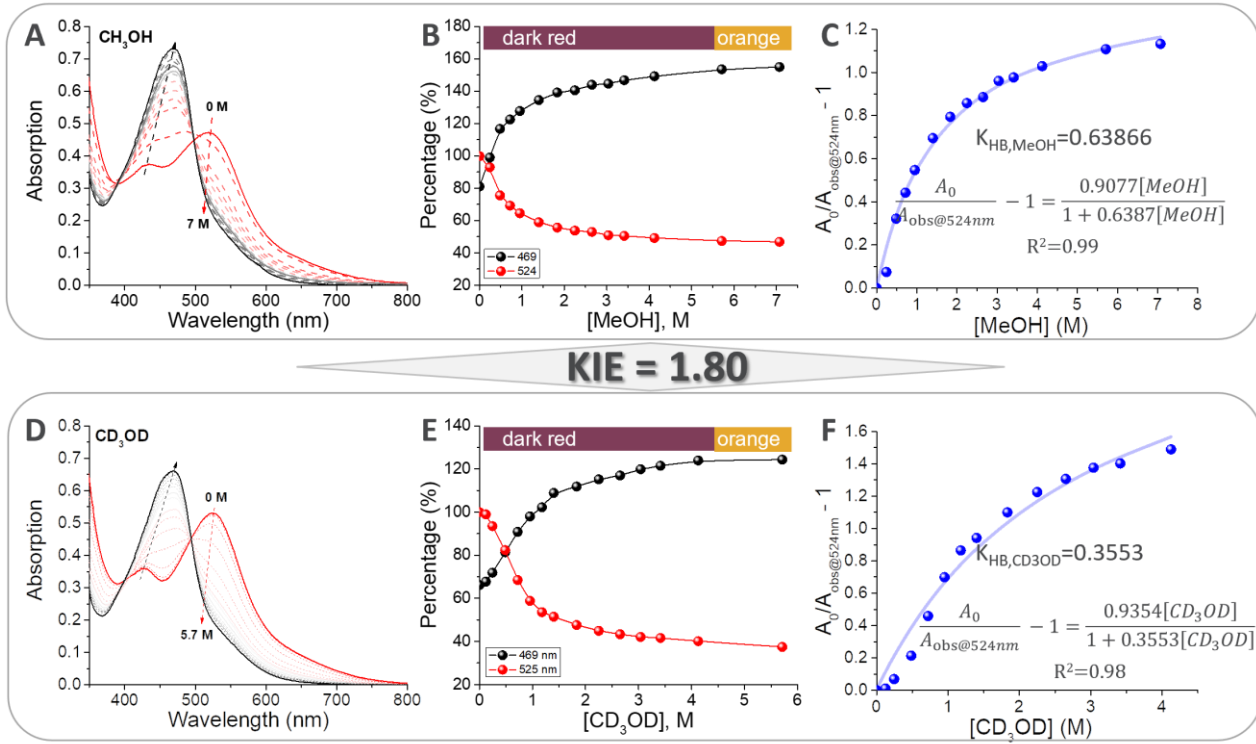


Fig. S 27. UV spectrum titration of 500 μM complexes Cu-4,7-CHO in acetone with adding (A) methanol and (D) methanol-d₄. (B, E) Absorption changes at 469 nm and 525 nm versus concentration (C, F) Plots of $(A_0/A_{\text{obs}} - 1)$ vs concentration of (C) methanol and (F) methanol-d₄, where A_0 is the absorption without adding methanol and A_{obs} is absorption with adding different amounts of methanol.

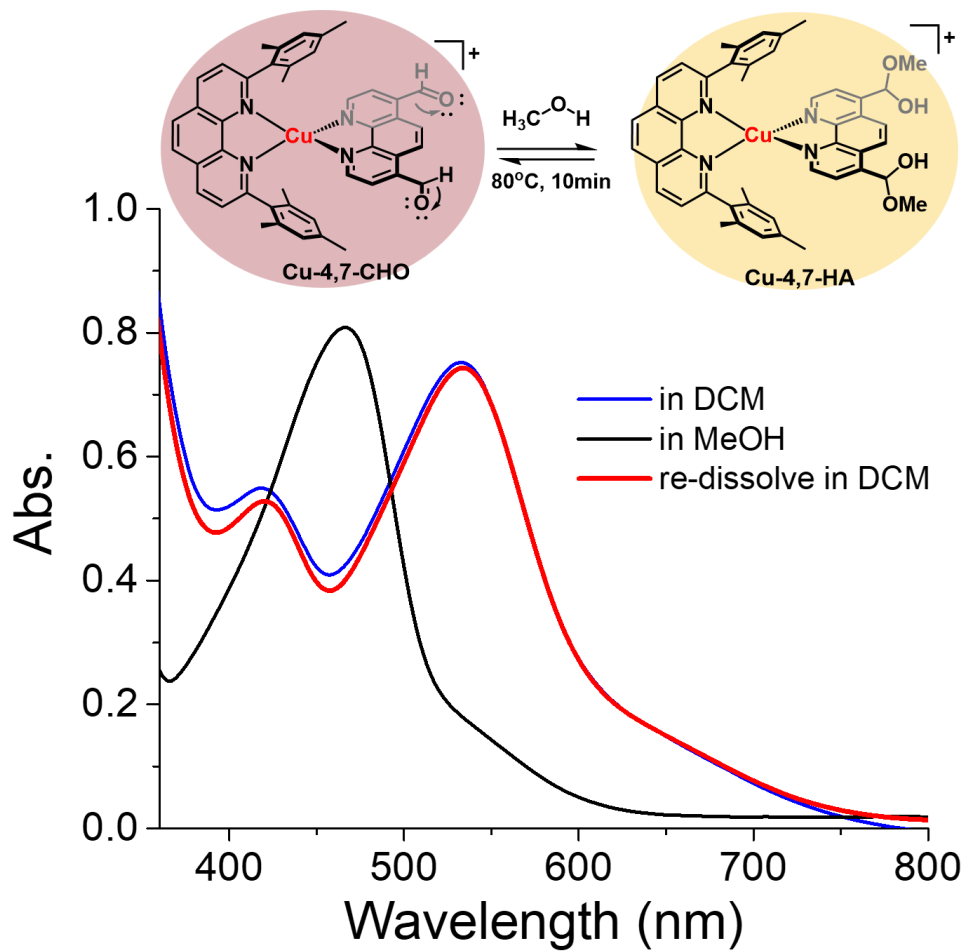


Figure S28. UV-Vis absorbance of complexes in dichloromethane, methanol, and then dry the methanol solution at 80°C for 10 min and re-dissolved it in dichloromethane.

References

- [1] T. Higashi, K. Inami and M. Mochizuki, *Journal of Heterocyclic Chemistry* **2008**, *45*, 1889-1892.
- [2] a) L. Kohler, D. Hayes, J. Hong, T. J. Carter, M. L. Shelby, K. A. Fransted, L. X. Chen and K. L. Mulfort, *Dalton Trans.* **2016**, *45*, 9871-9883; b) L. Kohler, R. G. Hadt, D. Hayes, L. X. Chen and K. L. Mulfort, *Dalton Trans.* **2017**, *46*, 13088-13100.
- [3] Z.-L. X. Lei Wang, Brian T. Phelan, Vincent M. Lynch, Lin X. Chen, Karen L. Mulfort, Changing direction: influence of ligand electronics on the directionality and kinetics of photoinduced charge transfer in Cu(I)diimine complexes, *Inorganic Chemistry* **2023**, accepted.
- [4] G. M. Sheldrick, *Acta Crystallographica Section A: Foundations and Advances* **2015**, *71*, 3-8.
- [5] G. M. Sheldrick, *Acta Crystallographica Section C: Structural Chemistry* **2015**, *71*, 3-8.
- [6] A. L. Spek, *Acta Crystallographica Section D: Biological Crystallography* **2009**, *65*, 148-155.
- [7] O. V. Dolomanov, L. J. Bourhis, R. J. Gildea, J. A. Howard and H. Puschmann, *Journal of applied crystallography* **2009**, *42*, 339-341.
- [8] A. J. C. Wilson and V. Geist in *International Tables for Crystallography. Volume C: Mathematical, Physical and Chemical Tables*. Kluwer Academic Publishers, Dordrecht/Boston/London 1992 (published for the International Union of Crystallography), 883 Seiten, ISBN 0 - 792 - 3 - 16 - 38X, Vol. Wiley Online Library, **1993**.
- [9] V. SHELXTL, Inc.: Madison, WI **1994**.
- [10] G. W. T. M. J. Frisch, H. B. Schlegel, G. E. Scuseria, M. A. Robb, J. R. Cheeseman, G. Scalmani, V. Barone, G. A. Petersson, H. Nakatsuji, X. Li, M. Caricato, A. V. Marenich, J. Bloino, B. G. Janesko, R. Gomperts, B. Mennucci, H. P. Hratchian, J. V. Ortiz, A. F. Izmaylov, J. L. Sonnenberg, D. Williams-Young, F. Ding, F. Lipparini, F. Egidi, J. Goings, B. Peng, A. Petrone, T. Henderson, D. Ranasinghe, V. G. Zakrzewski, J. Gao, N. Rega, G. Zheng, W. Liang, M. Hada, M. Ehara, K. Toyota, R. Fukuda, J. Hasegawa, M. Ishida, T. Nakajima, Y. Honda, O. Kitao, H. Nakai, T. Vreven, K. Throssell, J. Montgomery, J. A. J. E. Peralta, F. Ogliaro, M. J. Bearpark, J. J. Heyd, E. N. Brothers, K. N. Kudin, V. N. Staroverov, T. A. Keith, R. Kobayashi, J. Normand, K. Raghavachari, A. P. Rendell, J. C. Burant, S. S. Iyengar, J. Tomasi, M. Cossi, J. M. Millam, M. Klene, C. Adamo, R. Cammi, J. W. Ochterski, R. L. Martin, K. Morokuma, O. Farkas, J. B. Foresman and D. J. Fox, **2019**.
- [11] a) A. D. Beck, *J. Chem. Phys.* **1993**, *98*, 5648-5646; b) P. J. Stephens, F. J. Devlin, C. F. Chabalowski and M. J. Frisch, *The Journal of physical chemistry* **1994**, *98*, 11623-11627; c) C. Lee, W. Yang and R. G. Parr, *Physical review B* **1988**, *37*, 785.
- [12] P. J. Hay and W. R. Wadt, *The Journal of chemical physics* **1985**, *82*, 270-283.
- [13] a) P. C. Hariharan and J. A. Pople, *Theoretica chimica acta* **1973**, *28*, 213-222; b) W. J. Hehre, R. Ditchfield and J. A. Pople, *The Journal of Chemical Physics* **1972**, *56*, 2257-2261; c) R. Ditchfield, W. J. Hehre and J. A. Pople, *The Journal of Chemical Physics* **1971**, *54*, 724-728; d) M. M. Francz, W. J. Pietro, W. J. Hehre, J. S. Binkley, M. S. Gordon, D. J. DeFrees and J. A. Pople, *The Journal of Chemical Physics* **1982**, *77*, 3654-3665; e) T. Clark, J. Chandrasekhar, G. W. Spitznagel and P. V. R. Schleyer, *Journal of Computational Chemistry* **1983**, *4*, 294-301.
- [14] S. Miertuš, E. Scrocco and J. Tomasi, *Chemical Physics* **1981**, *55*, 117-129.
- [15] T. K. a. J. M. R. Dennington, **2008**.
- [16] R. L. Martin, *The Journal of chemical physics* **2003**, *118*, 4775-4777.
- [17] T. Lu and F. Chen, *Journal of computational chemistry* **2012**, *33*, 580-592.

- [18] a) W.-L. J. J. o. C. Weng and E. Data, **1999**, *44*, 63-66; b) M. Assael and S. J. I. J. o. T. Polimatiidou, **1994**, *15*, 95-107.
- [19] L. Hao, D. G. J. J. o. C. Leaist and E. Data, **1996**, *41*, 210-213.
- [20] A. Osatiashtiani, L. J. Durndell, J. C. Manayil, A. F. Lee and K. J. G. C. Wilson, **2016**, *18*, 5529-5535.